



# Effects of Si content on structure and soft magnetic properties of $\text{Fe}_{81.3}\text{Si}_x\text{B}_{17-x}\text{Cu}_{1.7}$ nanocrystalline alloys with pre-existing $\alpha$ -Fe nanocrystals

Xingjie Jia<sup>1,2</sup>, Wei Zhang<sup>2,\*</sup>, Yaqiang Dong<sup>1,3,\*</sup> , Aina He<sup>1,3</sup>, Jiawei Li<sup>1,3</sup>, and Run-Wei Li<sup>1,3</sup>

<sup>1</sup>Zhejiang Province Key Laboratory of Magnetic Materials and Application Technology, CAS Key Laboratory of Magnetic Materials and Devices, Ningbo Institute of Materials Technology & Engineering, Chinese Academy of Sciences, Ningbo 315201, Zhejiang, China

<sup>2</sup>Key Laboratory of Solidification Control and Digital Preparation Technology (Liaoning Province), School of Materials Science and Engineering, Dalian University of Technology, Dalian 116024, China

<sup>3</sup>University of Chinese Academy of Sciences, Beijing 100049, China

Received: 23 June 2020

Accepted: 29 September 2020

Published online:

9 October 2020

© Springer Science+Business Media, LLC, part of Springer Nature 2020

## ABSTRACT

The as-spun structure, thermal stability, crystallization structure and soft magnetic properties of  $\text{Fe}_{81.3}\text{Si}_x\text{B}_{17-x}\text{Cu}_{1.7}$  ( $x = 0-8$ ) alloys were investigated. The Fe–Si–B–Cu amorphous alloys contain  $\alpha$ -Fe nanocrystals with a high number density ( $N_d$ ) in as-spun state and show uniform nanocrystalline structure and typical soft magnetic characteristics after annealing. The rise of Si content from 0 to 4 at% increases the  $N_d$ , while the further rise to 8 at% shows an adverse effect. The increased  $N_d$  enhances competitive growth between the crystals during crystallization process, then refines structure and improves soft magnetic properties of the nanocrystalline alloys. Contrarily, the decreased  $N_d$  results in coarsened nanostructure and deteriorated magnetic softness. The alloy with Si content of 4 at% contains  $\alpha$ -Fe crystals with a high  $N_d$  of  $2.2 \times 10^{23} \text{ m}^{-3}$  in as-spun state and possesses fine  $\alpha$ -Fe grains with an average size ( $D$ ) of 14 nm, low coercivity ( $H_c$ ) of 7.1 A/m, high effective permeability (at 1 kHz) of 16,500 and saturation magnetic flux density of 1.77 T after annealing at 668 K for 60 min. In addition, the  $H_c$  of present Fe–Si–B–Cu nanocrystalline alloys is almost proportional to  $D^3$  due to the high ratio of uniaxial anisotropy to average random anisotropy.

Handling Editor: P. Nash.

Address correspondence to E-mail: wzhang@dlut.edu.cn; dongyq@nimte.ac.cn

<https://doi.org/10.1007/s10853-020-05404-w>

 Springer

## Introduction

Fe-based nanocrystalline soft magnetic alloys composed of nano-sized  $\alpha$ -Fe grains dispersing uniformly in residual amorphous phase have drawn considerable attention due to their excellent soft magnetic properties, such as, low coercivity ( $H_c$ ), low saturation magnetostriction, high permeability, and low core loss in high frequency, which basically originates from the low average random anisotropy ( $K_1$ ) achieved by the exchange interaction of the grains [1–4]. The Fe–Si–B–Nb–Cu nanocrystalline alloys (FINEMET) developed by Yoshizawa et al. have been widely used as magnetic cores because of their excellent soft magnetic softness and good manufacturability, while their low saturation magnetic flux density ( $B_s$ ) of 1.24 T is unfavorable for the miniaturization of the electromagnetic applications [1–5]. With the aim of promoting the energy conservation and miniaturization of the electromagnetic devices, much effort has been devoted in developing nanocrystalline alloys with high  $B_s$  and excellent magnetic softness [6–11]. The Fe–(Si, B, P, C)–Cu and Fe–B–(Cu) nanocrystalline alloys with high  $B_s$  of about 1.8 T, low  $H_c$  and core loss are successively developed in recent years, while most of them require a high heating rate annealing that is hard to achieve in industrial production to obtain the excellent magnetic softness [5, 10, 12–15], which hinder their industrialized applications.

Recently, we found that the rise of Cu content from 1.3 to 1.7 at% in melt-spun  $\text{Fe}_{83-x}\text{Si}_4\text{B}_{13}\text{Cu}_x$  alloys could generate  $\alpha$ -Fe nanocrystals with a high number density ( $N_d$ ), whose strong competitive growth could effectively hinder their overgrowth during annealing, hence the nanocrystalline alloy with fine  $\alpha$ -Fe grains and excellent soft magnetic properties can be obtained after a low heating rate annealing [16]. In this alloy system, the high Cu content of 1.7 at% plays the key role of promoting the nucleation during the formation of the pre-existing  $\alpha$ -Fe crystals [16–19] and the high Fe content provides the basis for the formation of the crystal, while the effects of the metalloid elements content are still no clear. The as-spun structure of multi-component alloys is also closely related to their amorphous forming ability (AFA). It has been reported that the Si could adjust the AFA without deteriorate their  $B_s$  [20–22] and promote the precipitation of  $\alpha$ -Fe phase in Fe-based

amorphous alloys [23], hence it's interesting to study its effects on the as-spun and crystallization structure of the Fe–Si–B–Cu alloys with pre-existing  $\alpha$ -Fe crystals. Besides, we also found that the relationship between  $H_c$  and average  $\alpha$ -Fe grains size ( $D$ ) of the  $\text{Fe}_{83-x}\text{Si}_4\text{B}_{13}\text{Cu}_x$  nanocrystalline alloys follows the law of  $H_c \propto D^3$  and shows a deviation in large- $D$  region [24]. The  $D^3$  law is first reported in Fe–Zr–B alloys, whose magnetization process is basically governed by strong uniaxial anisotropy ( $K_u$ ), which is different from the well-known  $D^6$  law for the Fe–Si–B–Nb–Cu alloys with magnetization process governed by average random anisotropy ( $K_1$ ) [25, 26].

In this work, we investigated the effects of Si content on as-spun structure, thermal stability, crystallization structure and soft magnetic properties of  $\text{Fe}_{81.3}\text{Si}_x\text{B}_{17-x}\text{Cu}_{1.7}$  ( $x = 0–8$ ) alloys and discussed the related mechanism in terms of the structure and crystallization process of as-spun alloys; summarized the correlation between structure and soft magnetic properties of the Fe–Si–B–Cu nanocrystalline alloys and clarified its root by estimating their  $K_u$  and  $K_1$ .

## Experimental procedure

Alloy ingots with nominal compositions of  $\text{Fe}_{81.3}\text{Si}_x\text{B}_{17-x}\text{Cu}_{1.7}$  ( $x = 0–8$ ) were prepared by alloying Fe (99.95 mass %), Si (99.999 mass %), B (99.9 mass %) and Cu (99.99 mass %) in an arc melting furnace under an argon atmosphere. The mass losses were less than 0.2 mass%. Ribbon samples with a width of about 1.5 mm and thickness of about 20  $\mu\text{m}$  were prepared by single roller melt-spinning under an argon atmosphere. The as-spun ribbons were sealed in a vacuumed quartz tube, and isothermally annealed in a muffle furnace for 60 min under a heating rate of about 20  $\text{K min}^{-1}$  followed by water quenching. The thermal properties of as-spun alloys were investigated by a differential scanning calorimetry (DSC, TA Instruments Q20) under a heating rate of 40  $\text{K min}^{-1}$ . The structure of the samples was examined by X-ray diffraction (XRD, Bruker D8 Focus) with Cu  $K\alpha$  radiation and transmission electron microscopy (TEM, JEOL JEM-2100F). The XRD and TEM experiments were performed on air side and middle part of the ribbons, respectively. The  $D$  of the  $\alpha$ -Fe grains was estimated by using Scherrer formula from the full width at half

maximum of the (110) peak in XRD patterns or fitting the size distribution of the grains in a selected TEM image. The  $N_d$  of the crystals was estimated by  $N_d = N/(A \times D)$ , where  $N$  is quantity of the grains and  $A$  is the area of the TEM image [17]. The volume fraction of  $\alpha$ -Fe phase ( $V_{cry}$ ) was estimated by using  $V_{cry} = N_d \pi D^3/6$  or  $V_{cry} = I_{cry}/(I_{cry} + I_{amo})$ , where  $I_{cry}$  and  $I_{amo}$  are the integral intensities of diffraction peaks of crystalline and amorphous phase determined from the XRD patterns, respectively [16, 27–29]. The  $B_s$  was measured by a vibrating sample magnetometer (VSM, Lake Shore 7410) under a maximum applied field of  $800 \text{ kA m}^{-1}$ . The  $H_c$  and initial magnetization curve were measured using straight ribbons with a length of 60 mm by a dc  $B$ - $H$  loop tracer (Linkjoin MATS-2010SD) under an applied field of  $4000 \text{ A/m}$ . The effective permeability ( $\mu_e$ ) was measured by an impedance analyzer (Agilent 4294A) under an applied field of  $1 \text{ A/m}$  and frequency of  $1 \text{ kHz}$ . The density was measured by the Archimedeian method using diethyl terephthalate.

### Results and discussion

Figure 1 shows the XRD patterns of the as-spun  $\text{Fe}_{81.3}\text{Si}_x\text{B}_{17-x}\text{Cu}_{1.7}$  ( $x = 0$ –8) alloys. The patterns of the  $x = 0$ –8 alloys contain of only broad peaks, indicating an amorphous feature. The bright-field TEM images, corresponding selected area electron diffraction (SAED) patterns and gain size distributions (the red

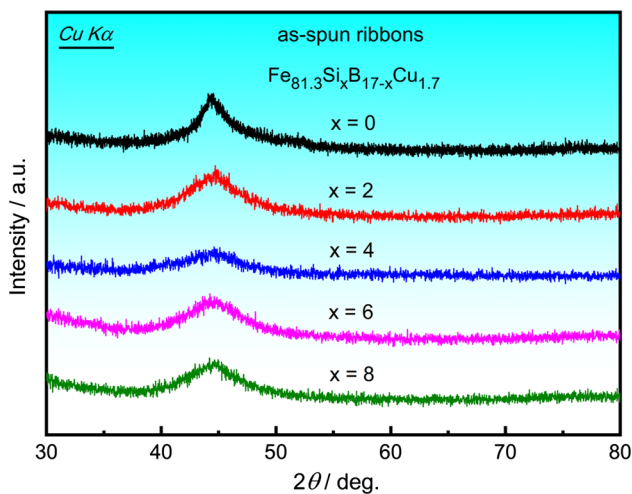


**Figure 1** XRD patterns of as-spun  $\text{Fe}_{81.3}\text{Si}_x\text{B}_{17-x}\text{Cu}_{1.7}$  ( $x = 0$ –8) alloys.

lines show the normal distribution, the numbers are the desired value and standard deviation, respectively) of the as-spun  $\text{Fe}_{81.3}\text{Si}_x\text{B}_{17-x}\text{Cu}_{1.7}$  ( $x = 0, 4, 8$ ) alloys are shown in Fig. 2. All alloys possess the composite structure of  $\alpha$ -Fe crystals (identified by the corresponding SAED patterns) dispersing in amorphous phase. The variations in  $N_d$ ,  $D$  and  $V_{cry}$  of the  $\alpha$ -Fe crystals as a function of Si content are exhibited in Fig. 3. The  $N_d$  and  $D$  of the crystals in the  $x = 0$  alloy were measured as  $9.7 \times 10^{22} \text{ m}^{-3}$  and  $10.0 \text{ nm}$ , respectively. The rise of Si content to 4 at% increases the  $N_d$  to  $2.2 \times 10^{23} \text{ m}^{-3}$  and decreases the  $D$  to  $6.2 \text{ nm}$ , suggesting that a proper amount of Si facilitates the formation of  $\alpha$ -Fe crystals with a high  $N_d$  and small  $D$ ; the further rise of Si content to 8 at% decreases the  $N_d$  and  $D$  to  $1.1 \times 10^{22} \text{ m}^{-3}$  and  $5.0 \text{ nm}$ , respectively, demonstrating that the excessive Si suppresses the precipitation of  $\alpha$ -Fe crystals during melt-spinning. The rise of Si content from 0 to 8 at% lowers the  $V_{cry}$  from 5.1 to 0.1%, indicating the enhancement of the AFA. We also noticed that the standard deviations for the  $x = 0, 4$  and  $8$  alloys are 2.6, 1.0 and 1.2, respectively, which suggest that the  $\alpha$ -Fe crystals in  $x = 4$  and  $8$  alloys are more uniform than that of the  $x = 0$  alloy. In addition, the difference between the XRD and TEM results may originate from the quite small  $D$  and low  $V_{cry}$  of  $\alpha$ -Fe phase, which cannot be detected by the XRD, especially for the  $x = 2$ –8 alloys [16, 18].

It's well known that certain atomic-size mismatch and large negative mixing enthalpy could enhance the AFA of a multi-component alloy system [30, 31]. For the Fe–Si–B–Cu alloys, the addition of Si could produce the proper mismatch of atomic sizes (Cu:  $0.128 \text{ nm}$ , Fe:  $0.124 \text{ nm}$ , Si:  $0.115 \text{ nm}$ ; B:  $0.82 \text{ nm}$  [32]) and then induce an increased atomic packing degree of the liquid state, which is always associated with low free energy, higher density and viscosity of the liquid alloys [30, 31], hence facilitates the formation of amorphous phase. The mixing enthalpy of an alloy system can be determined by the following equation:

$$\Delta H_{\text{mix}} = \sum_{i=1, j > i}^n 4\Delta H_{AB}^{\text{mix}} C_i C_j \quad (1)$$

where  $\Delta H_{AB}^{\text{mix}}$  is the mixing enthalpy for binary AB alloy with equal atomic ratio, and  $c_i$  and  $c_j$  are percentage of different elements [33]. The presence of Si causes the generation of strong chemical affinities with large negative mixing enthalpy, i.e., Fe–Si

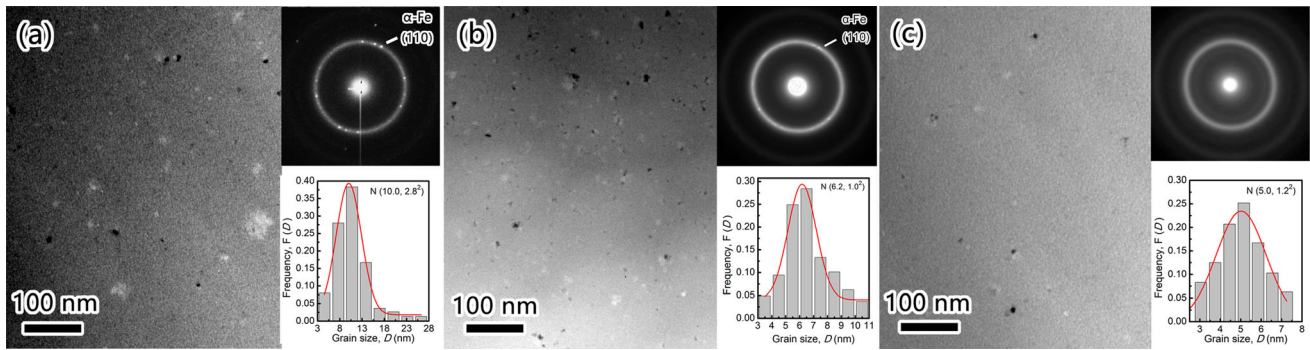


**Figure 2** Bright-field TEM images, corresponding SAED patterns and grain size distributions of as-spun  $\text{Fe}_{81.3}\text{Si}_x\text{B}_{17-x}\text{Cu}_{1.7}$  alloys. **a:**  $x = 0$ , **b:**  $x = 4$ , **c:**  $x = 8$ .

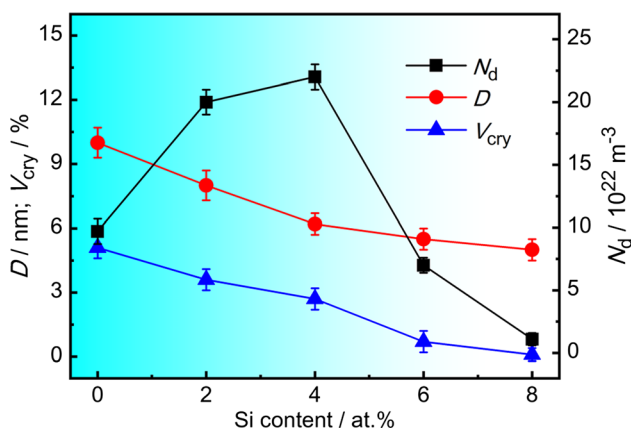


**Figure 3** The variations in  $N_d$ ,  $D$  and  $V_{\text{cry}}$  as a function of Si content for  $\alpha\text{-Fe}$  crystals in as-spun  $\text{Fe}_{81.3}\text{Si}_x\text{B}_{17-x}\text{Cu}_{1.7}$  ( $x = 0\text{--}8$ ) alloys.

( $-35 \text{ kJ/mol}$ ), Si–B ( $-14 \text{ kJ/mol}$ ) and Si–Cu ( $-19 \text{ kJ/mol}$ ) [34], thus the rise of Si content from 0 to 8 at% in the Fe–Si–B–Cu alloys decreases the  $\Delta H_{\text{mix}}$  from  $-13.7$  to  $-16.5 \text{ kJ/mol}$ , which is conducive to amorphous formation. As discussed above, the rise of Si content could improve the AFA of the Fe–Si–B–Cu alloys and retard the precipitation of crystal phase during melt-spinning, hence the  $V_{\text{cry}}$  of  $\alpha\text{-Fe}$  crystal in the as-spun alloys decreases gradually. For the  $x = 0$  alloy, once some  $\alpha\text{-Fe}$  crystals is formed, they will growth rapidly due to the poor AFA, and then other crystals are unable to form due to the dilution of Fe atoms, thus the  $\alpha\text{-Fe}$  crystals in the as-spun alloy possess a low  $N_d$  and large  $D$ . The rise of Si content to 4 at% enhance the AFA, hence the growth of the  $\alpha\text{-Fe}$  crystals is restrained during melt-spinning. Eventually, the  $\alpha\text{-Fe}$  crystals with a high  $N_d$  and small  $D$  are formed under the combined action of the high Cu content and the sufficient high AFA. The rise of Si content to 8 at% improves the AFA further, and then

the formation of the  $\alpha\text{-Fe}$  crystals are suppressed strongly, thus the  $N_d$  and  $D$  are decreased.

DSC curves of as-spun  $\text{Fe}_{81.3}\text{Si}_x\text{B}_{17-x}\text{Cu}_{1.7}$  ( $x = 0\text{--}8$ ) alloys are exhibited in Fig. 4. All alloys have 2 overlapped exothermic peaks (the onset temperatures are marked as  $T_{x1}$ ) that corresponding to the growth of the pre-existing  $\alpha\text{-Fe}$  crystals and subsequent nucleation and growth of new  $\alpha\text{-Fe}$  crystals [24], which followed by exothermic peaks (the onset temperatures are marked as  $T_{x2}$ ) resulting from the formations of non-soft magnetic phases like iron–boride [5, 10, 12]. The rise of Si content from 0 to 4 at% decreases  $T_{x1}$  from 652 to 634 K and the further rise of Si content to 8 at% increases the  $T_{x1}$  to 639 K, suggesting that the a proper amount of Si promotes the growth of the pre-existing  $\alpha\text{-Fe}$  crystals and the excessive Si shows an opposite effect. The rise of Si content from 0 to 8 at% increases the  $T_{x2}$  from 739 to 817 K gradually, illustrating that the precipitations of

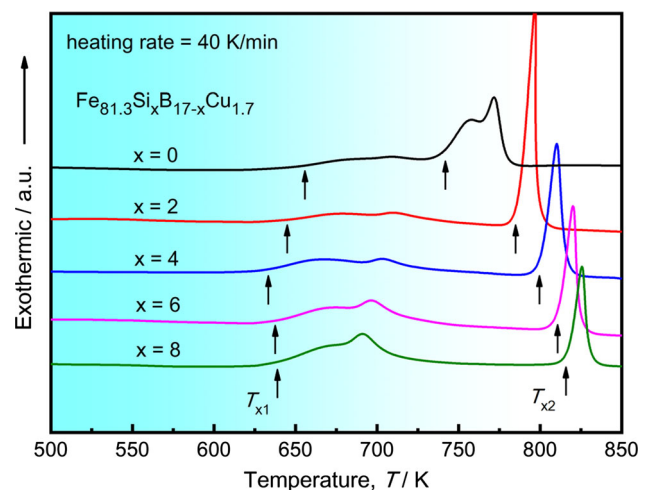


**Figure 4** DSC curves of as-spun  $\text{Fe}_{81.3}\text{Si}_x\text{B}_{17-x}\text{Cu}_{1.7}$  ( $x = 0\text{--}8$ ) alloys.

iron–boride phases are suppressed. In addition, the rise of Si content shifts the exothermic peaks corresponding to the precipitation of iron–boride phase from two to one, suggesting the crystallization process of the residual amorphous phase is changed.

The thermal stability of the as-spun Fe–Si–B–Cu alloys is closely related to their structure. The rise of Si content from 0 to 4 at% lowers the  $V_{\text{cry}}$  and  $D$ , then the abundant Fe atoms around the pre-existing  $\alpha$ -Fe crystals makes them easier to growth, hence the  $T_{x1}$  decreases gradually. The further rise of Si content to 8 at% enhances AFA of the alloys, which will significantly inhibit the long-range diffusion of Fe atoms, thus the growth of the pre-existing  $\alpha$ -Fe crystals is restrained and then the  $T_{x1}$  goes up again. The increased  $T_{x2}$  of the Si-containing alloys can be attributed to the competitive growth of several crystal phases and their complicated crystalline structure [23, 35]. Besides, Si and B have a large negative mixing enthalpy of  $-14$  kJ/mol [34], thus the strong chemical affinity between B and Si may inhibit the diffusion of B atoms, then inhibit the precipitation of iron–boride and promote the thermal stability of the residual amorphous phase.

Figure 5 shows the XRD patterns of the  $\text{Fe}_{81.3}\text{Si}_x\text{B}_{17-x}\text{Cu}_{1.7}$  ( $x = 0-8$ ) alloys annealed at optimum annealing temperature ( $T_a$ ), defined from the temperature at which the lowest  $H_c$  and high  $B_s$  were obtained simultaneously. The alloys with more Si possess higher optimum  $T_a$  due to their increased  $T_{x2}$ . The single  $\alpha$ -Fe phase was precipitated in all annealed alloys. The bright-field TEM images, corresponding

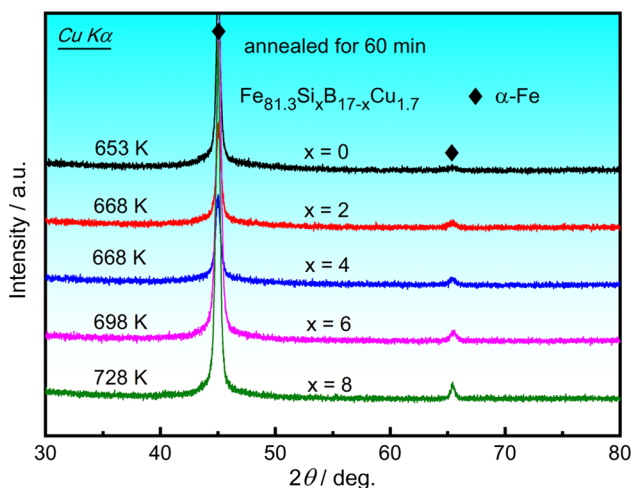


**Figure 5** XRD patterns of  $\text{Fe}_{81.3}\text{Si}_x\text{B}_{17-x}\text{Cu}_{1.7}$  ( $x = 0-8$ ) alloys annealed at optimum  $T_a$  for 60 min.

SAED patterns and grain size distributions of the annealed  $\text{Fe}_{81.3}\text{Si}_x\text{B}_{17-x}\text{Cu}_{1.7}$  ( $x = 0, 4, 8$ ) alloys are shown in Fig. 6. The nanocrystalline structure composed of  $\alpha$ -Fe grains uniformly dispersing in residual amorphous phase is obtained in all alloys. The variations in  $D$ ,  $N_d$  and  $V_{\text{cry}}$  as a function of Si content for  $\alpha$ -Fe grains in the annealed  $\text{Fe}_{81.3}\text{Si}_x\text{B}_{17-x}\text{Cu}_{1.7}$  ( $x = 0-8$ ) alloys are exhibited in Fig. 7. The rise of Si content from 0 to 4 at% decreases the  $D$  from 18.8 to 14.0 nm and increases  $N_d$  from  $1.1 \times 10^{23}$  to  $2.8 \times 10^{23} \text{ m}^{-3}$ , and then the further rise of Si content to 8 at% increases the  $D$  to 34.2 nm and lowers the  $N_d$  to  $1.8 \times 10^{22} \text{ m}^{-3}$ . The XRD and TEM results suggest that the rise of Si content from 0 to 4 at% refines the  $\alpha$ -Fe grains, while the further rise of Si content coarsens the nanostructure. Besides, the  $x = 0$  alloy possesses a smaller  $V_{\text{cry}}$  of 47% than that of 49–50% for the  $x = 4-8$  alloy (see Fig. 7), which may result from its relatively low optimum  $T_a$ . In addition, we noticed that the rise of Si content in  $\text{Fe}_{81.3}\text{Si}_x\text{B}_{17-x}\text{Cu}_{1.7}$  alloys increases the peak position of (110) for the  $\alpha$ -Fe phase from  $44.85^\circ$  to  $45.23^\circ$ , revealing the decrease of plane distance, which may results from the solution of Si atoms. Actually, Si always solutes into  $\alpha$ -Fe phase in Fe-based nanocrystalline alloys, and the phenomenon has been reported in Fe–Si–B–Nb–Cu and Fe–Si–B–P–Cu alloy systems [2, 23].

Based on the structure of as-spun and annealed alloys, we propose a reasonable model to describe the crystallization process of the Fe–Si–B–Cu alloys with various Si content, as shown in Fig. 8. Due to the pre-existing  $\alpha$ -Fe crystals in the as-spun alloys, the formation of the Fe–Si–B–Cu nanocrystalline alloys contains the growth of pre-existing  $\alpha$ -Fe crystals and subsequent nucleation and growth of the new  $\alpha$ -Fe crystals [16, 24]. For the  $x = 0$  alloy, the pre-existing  $\alpha$ -Fe crystals have a relatively low  $N_d$  and large  $D$  due to the poor AFA, meanwhile, the  $N_d$  of the newly formed crystals is also very low due to the low heating rate. The competitive growth between the pre-existing and newly–formed crystals couldn't suppress the growth of  $\alpha$ -Fe grains, which results in the relatively large  $\alpha$ -Fe grains in the annealed alloy (see A1–A3 in Fig. 8). For the  $x = 4$  alloy, the pre-existing  $\alpha$ -Fe crystals have a high  $N_d$ , the competitive growth between them can inhibit their excessive growth effectively. During annealing, some new crystals will form and the harmonious growth of the pre-existing and newly formed crystals results in the uniform and fine nanostructure of the annealed alloy

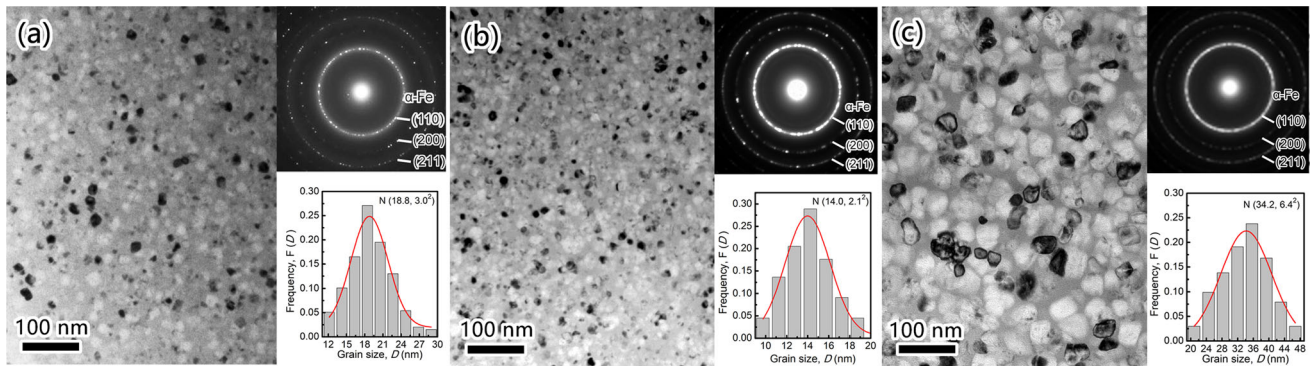


**Figure 6** Bright-field TEM images, corresponding SAED patterns and grain size distributions of the annealed  $\text{Fe}_{81.3}\text{Si}_x\text{B}_{17-x}\text{Cu}_{1.7}$  alloys. **a:**  $x = 0$ , **b:**  $x = 4$ , **c:**  $x = 8$ .

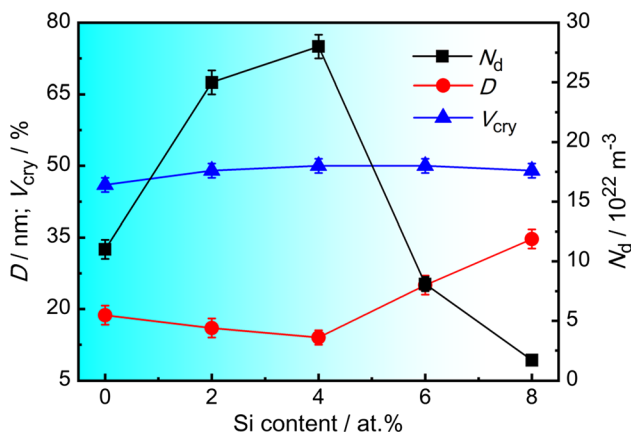


**Figure 7** The variations in  $D$ ,  $N_d$  and  $V_{\text{cry}}$  as a function of Si content for  $\alpha$ -Fe grains in the annealed  $\text{Fe}_{81.3}\text{Si}_x\text{B}_{17-x}\text{Cu}_{1.7}$  ( $x = 0$ –8) alloys.

(see B1–B3 in Fig. 8). For the  $x = 8$  alloy, the pre-existing and newly-formed crystals have a very low  $N_d$ , they will grow up freely due to the absence of competitive growth, hence the annealed alloys have coarse  $\alpha$ -Fe grains (see C1–C3 in Fig. 8).

Figure 9 exhibits the variations in  $H_c$ ,  $\mu_e$  and  $B_s$  as a function of Si content for  $\text{Fe}_{81.3}\text{Si}_x\text{B}_{17-x}\text{Cu}_{1.7}$  ( $x = 0$ –8) alloys. The rise of Si content from 0 to 4 at% decreases the  $H_c$  from 27.3 to 7.1 A/m, increases the  $\mu_e$  and  $B_s$  from 7000 and 1.73 T to 16,500 and 1.77 T respectively, illustrating the great refinement of nanostructure and improvement of magnetic properties; the further rise of Si content to 8 at% increases the  $H_c$  to 67.9 A/m, decreases the  $\mu_e$  and  $B_s$  to 1200 and 1.76 T, respectively, suggesting the coarsening of nanocrystalline structure and deterioration of magnetic softness. The soft magnetic properties of Fe-based nanocrystalline alloys have a significant correlation with the structure. According to the random

anisotropy model, the intergranular exchange coupling between the  $\alpha$ -Fe grains could minimize the effect of the magneto-crystalline anisotropy ( $K$ ) when the  $D$  is smaller than the exchange-coupled length ( $L_0$ , 30–40 nm), thus the alloys with finer  $\alpha$ -Fe grains possess improved magnetic softness [26]. The rise of Si content from 0 to 4 at% refines the  $\alpha$ -Fe grains, and thus the  $H_c$  is lowered and the  $\mu_e$  is increased; the further rise of Si content to 8 at% coarsens the grains, hence the  $H_c$  increases and  $\mu_e$  decreases gradually. The  $B_s$  of Fe-based nanocrystalline alloys is expressed as:

$$B_s = B_{\text{sc}} V_{\text{cry}} + B_{\text{sa}} (1 - V_{\text{cry}}) \quad (2)$$

where  $B_{\text{sc}}$  and  $B_{\text{sa}}$  are saturation magnetic flux density of crystal and amorphous phase, respectively [36]. The XRD and TEM results suggest that the rise of Si content from 0 to 4–8 increases the  $V_{\text{cry}}$  slightly, hence the  $x = 4$ –8 nanocrystalline alloys show higher  $B_s$  of 1.76–1.77 T as compared with that of 1.73 T for  $x = 0$  alloy. In addition, the rise of Si content from 4 to 8 at% slightly decreases the  $B_s$  from 1.77 to 1.76 T, which may result from the solution of Si in the  $\alpha$ -Fe grains [37–39].

We also analyzed the correlation between the  $H_c$  and  $D$  of the Fe–Si–B–Cu alloys, which is found to follow the  $D^3$  law. Zang et al. and Sharma et al. also reported similar results in small- $D$  region for Fe–B–(Cu) and Fe–Si–B–P–Cu alloys [14, 40], which seems to be a common phenomenon for Fe-based nanocrystalline alloys with high Fe content. It has been reported that the correlation will change from  $D^6$  to  $D^3$  law when the  $K_u/K_1$  exceeds approximately 2 to 1 [41]. With the aim of further understanding the correlation of the Fe–Si–B–Cu alloys, we calculated the

**Figure 8** Schematic illustrations for crystallization process of Fe<sub>81.3</sub>Si<sub>x</sub>B<sub>17-x</sub>Cu<sub>1.7</sub> alloys.

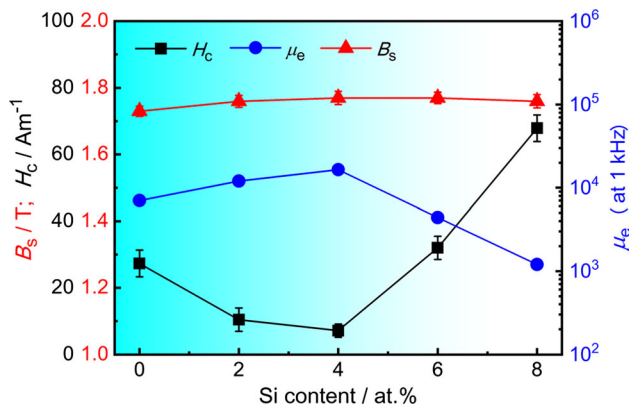
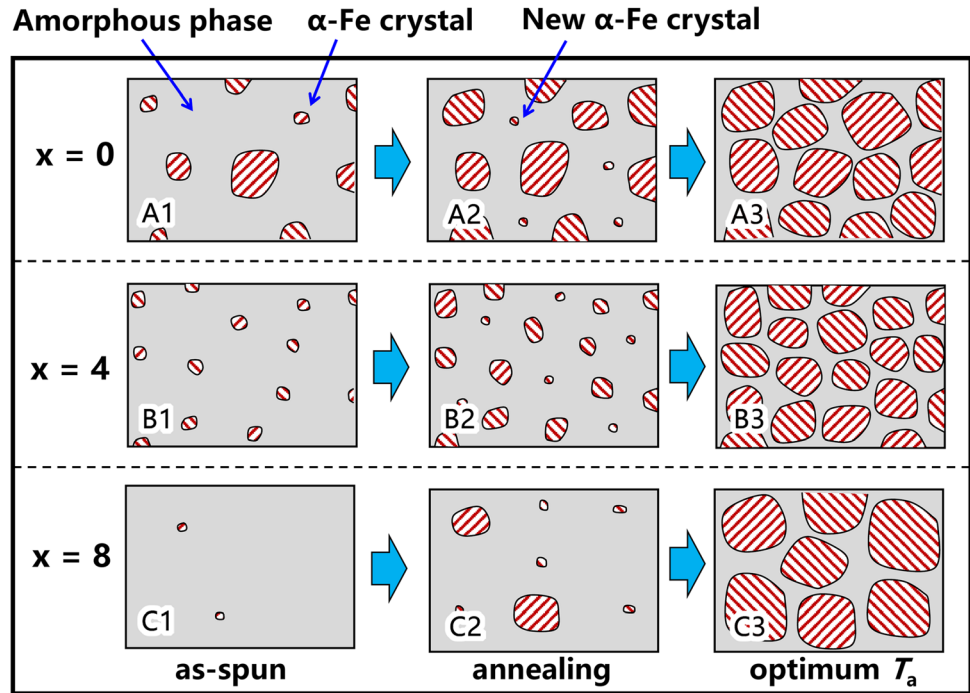


**Figure 9** The variations in  $H_c$ ,  $\mu_e$  and  $B_s$  as a function of Si content for the annealed Fe<sub>81.3</sub>Si<sub>x</sub>B<sub>17-x</sub>Cu<sub>1.7</sub> alloys.

$K_1$  and  $K_u$  of present Fe–Si–B–Cu nanocrystalline alloys. The  $K_1$  can be calculated by the expression:

$$K_1 = \beta KV_{\text{cry}}^2 (D/L_0)^6 \tag{3}$$

where  $\beta$  is anisotropy constant, which is 0.4 for cubic system [42], and then the  $K_1$  are estimated as 43, 15, 6, 143 and 724 J/m<sup>3</sup> for the  $x = 0, 2, 4, 6$  and 8 alloys, respectively (see the computational process in Appendix). The  $K_u$  was estimated by the expression:

$$K_u = B_s H_k / 2 \tag{4}$$

where  $H_k$  is the applied field strength at the intercept between  $B_s$  and a tangent line drawn from the

gradient of the initial magnetization [43], and then the  $K_u$  are calculated as  $84 \pm 4, 35 \pm 3, 23 \pm 2, 97 \pm 5$  and  $121 \pm 7$  J/m<sup>3</sup> for the  $x = 0, 2, 4, 6$  and 8 alloys, respectively (see the computational process in Appendix). Parsons et al. reported the  $K_u$  of Fe–Si–B–Cu nanocrystalline alloys with  $D$  of 18–26 nm and  $H_c$  of 12–15 A/m is measured as about 40–69 J/m<sup>3</sup> [43], which is quite close to that of 35–84 J/m<sup>3</sup> for the  $x = 0$  and 2 alloys with similar structure and magnetic properties. Zang et al. reported that the  $K_u$  of Fe–B(–Cu) nanocrystalline alloys with  $H_c$  of about 10 A/m could be estimated as 20 J/m<sup>3</sup> [40], which is much alike with than of 23 J/m<sup>3</sup> of the  $x = 4$  alloy with a  $H_c$  of 7.1 A/m. Based on the calculated  $K_1$  and  $K_u$  value, the  $K_u/K_1$  is determined as about 1.47–3.83 for the  $x = 0–6$  alloys, suggesting the  $K_u$  basically governs the magnetization process, hence the  $H_c$  and  $D$  of present alloys follow the  $D^3$  law. Besides, the  $K_u/K_1$  of the  $x = 8$  alloy is 0.17, which means the magnetization process is governed by the  $K_1$ , then the correlation may change to  $D^6$  law if  $D$  increases further. Actually, this change does exist in large- $D$  region of Fe–B(–Cu), Fe–Si–B–P–Cu and Fe–Si–B–Cu alloys [14, 24, 40]. It should be noticed that the change point for the Fe–B(–Cu) and Fe–Si–B–P–Cu alloys are about 30–35 nm and 25 nm, respectively [14, 40], while it may be about 40–50 nm for the Fe–Si–B–Cu alloys

with pre-existing  $\alpha$ -Fe nanocrystals [24], and the root of this obvious difference needs to be studied further.

The presence of  $K_u$  has a great influence on magnetic softness of Fe-based nanocrystalline alloys, hence it is significant to clarify the origin of the relatively large  $K_u$  of present Fe–Si–B–Cu alloys. The three-dimensional atom probe analyses in our previous work suggest a small amount of B atoms dissolved in the  $\alpha$ -Fe crystal phase of the Fe–Si–B–Cu alloys [24]. The annealing temperatures (653–728 K) are well below the Curie point of the  $\alpha$ -Fe phase (1043 K), hence the local spontaneous magnetization could produce the directional atomic order ordering of solute atoms in the crystal phase, which will produce field-induced  $K_u$  in the Fe-based nanocrystalline alloys [41]. The residual compressive stress in the surfaces of the annealed alloys also could generate the stress-induced  $K_u$  [42]. It has been reported that the complete release of the compressive stress in a melt-spun Fe<sub>79</sub>B<sub>16</sub>Si<sub>5</sub> ribbon surface requires annealing at 673 K for 420 min [44]. The Fe–Si–B–Cu nanocrystalline alloys are obtained by annealing at 653–728 K for 60 min, thus the residual stress is believed to still exist. In general, the  $K_u$  in the Fe–Si–B–Cu nanocrystalline alloys may originate from the combined action of solution of B atoms and residual compressive stress.

## Conclusion

The effects of Si content on the as-spun structure, thermal stability, crystallization structure and soft magnetic properties of Fe<sub>81.3</sub>Si<sub>x</sub>B<sub>17-x</sub>Cu<sub>1.7</sub> ( $x = 0$ –8) alloys were investigated and the related mechanism was discussed. The results are summarized as follows:

1. The rise of  $x$  from 0 to 4 at% increases  $N_d$  of pre-existing  $\alpha$ -Fe crystals from  $9.7 \times 10^{22}$  to  $2.2 \times 10^{23} \text{ m}^{-3}$ , decreases  $D$  and  $V_{\text{cry}}$  from 10.0 nm and 5.1% to 6.2 nm and 2.7%, respectively, and lowers  $T_{x1}$  from 652 to 634 K; the further rise of  $x$  to 8 at% decreases  $N_d$ ,  $D$  and  $V_{\text{cry}}$  to  $1.1 \times 10^{22} \text{ m}^{-3}$ , 5.0 nm and 0.1%, respectively, and increases  $T_{x1}$  to 639 K.
2. The increased  $N_d$  enhances competitive growth between the crystals during crystallization process and then refines nanostructure and improves magnetic softness, hence the  $x = 4$  alloy possesses
3. The  $x = 4$ –8 nanocrystalline alloys exhibit higher  $B_s$  of 1.76–1.77 T than that of 1.73 T for the  $x = 0$  alloy due to increased  $V_{\text{cry}}$  of  $\alpha$ -Fe phase. The  $H_c$  of present Fe–Si–B–Cu nanocrystalline alloys is almost proportional to  $D^3$ , which may originates from the high ratio of  $K_u$ – $K_1$ .

## Acknowledgements

This research was supported by the National Key Research and Development Program of China [Grant No. 2016YFB0300500], the National Natural Science Foundation of China [Grant No. 51571047], Ningbo Major Special Projects of the Plan “Science and Technology Innovation 2025” [Grant No. 2018B10084].

## Compliance with ethical standards

**Conflict of interest** The authors declare that they have no conflict of interest.

**Electronic supplementary material:** The online version of this article (<https://doi.org/10.1007/s10853-020-05404-w>) contains supplementary material, which is available to authorized users.

## References

- [1] Herzer G (2013) Modern soft magnets: amorphous and nanocrystalline materials. *Acta Mater* 61:718–734. <https://doi.org/10.1016/j.actamat.2012.10.040>
- [2] Yoshizawa Y, Oguma S, Yamauchi K (1988) New Fe-based soft magnetic alloys composed of ultrafine grain structure. *J Appl Phys* 64:6044–6046. <https://doi.org/10.1063/1.342149>
- [3] McHenry ME, Willard MA, Laughlin DE (1999) Amorphous and nanocrystalline materials for applications as soft magnets. *Prog Mater Sci* 44:291–433. [https://doi.org/10.1016/S0079-6425\(99\)00002-X](https://doi.org/10.1016/S0079-6425(99)00002-X)

- [4] Yoshizawa Y (2001) Magnetic properties and applications of nanostructured soft magnetic materials. *Scripta Mater* 44:1321–1325. [https://doi.org/10.1016/s1359-6462\(01\)00700-x](https://doi.org/10.1016/s1359-6462(01)00700-x)
- [5] Makino A (2012) Nanocrystalline soft magnetic Fe-Si-BP-Cu alloys with high  $B$  of 1.8–1.9T contributable to energy saving. *IEEE Trans Magn* 48:1331–1335. <https://doi.org/10.1109/tmag.2011.2175210>
- [6] Makino A, Men H, Kubota T, Yubuta K, Inoue A (2009) FeSiBPCu nanocrystalline soft magnetic alloys with high  $B_s$  of 1.9 tesla produced by crystallizing hetero-amorphous phase. *Mater Trans JIM* 50:204–209. <https://doi.org/10.2320/matertrans.MER2008306>
- [7] Suzuki K, Kataoka N, Inoue A, Makino A, Masumoto T (1990) High saturation magnetization and soft magnetic properties of bcc Fe–Zr–B alloys with ultrafine grain structure. *Mater Trans JIM* 31:743–746. <https://doi.org/10.2320/matertrans1989.31.743>
- [8] Willard MA, Laughlin DE, McHenry ME, Thoma D, Sickafus K, Cross JO, Harris VG (1998) Structure and magnetic properties of  $(\text{Fe}_{0.5}\text{Co}_{0.5})_{88}\text{Zr}_7\text{B}_4\text{Cu}_1$  nanocrystalline alloys. *J Appl Phys* 84:6773–6777. <https://doi.org/10.1063/1.369007>
- [9] Ohta M, Yoshizawa Y (2008) Cu addition effect on soft magnetic properties in Fe–Si–B alloy system. *J Appl Phys* 103:07E722–13. <https://doi.org/10.1063/1.2829240>
- [10] Makino A, Kubota T, Yubuta K, Inoue A, Urata A, Masumoto H, Yoshida S (2011) Low core losses and magnetic properties of  $\text{Fe}_{85-86}\text{Si}_{1-2}\text{B}_8\text{P}_4\text{Cu}_1$  nanocrystalline alloys with high  $B$  for power applications. *J Appl Phys* 109:07A302–15. <https://doi.org/10.1063/1.3535169>
- [11] Zhang Y, Sharma P, Makino A (2014) Effects of cobalt addition in nanocrystalline  $\text{Fe}_{83.3}\text{Si}_4\text{B}_8\text{P}_4\text{Cu}_{0.7}$  soft magnetic alloy. *IEEE Trans Magn* 50:2003004–2003014. <https://doi.org/10.1109/TMAG.2013.2286617>
- [12] Sharma P, Zhang X, Zhang Y, Makino A (2015) Competition driven nanocrystallization in high  $B_s$  and low coreloss Fe-Si-B-P-Cu soft magnetic alloys. *Scripta Mater* 95:3–6. <https://doi.org/10.1016/j.scriptamat.2014.08.023>
- [13] Suzuki K, Parsons R, Zang BW, Onodera K, Kishimoto H, Kato A (2017) Copper-free nanocrystalline soft magnetic materials with high saturation magnetization comparable to that of Si steel. *Appl Phys Lett* 110:012407–12414. <https://doi.org/10.1063/1.4973772>
- [14] Zang BW, Parsons R, Onodera K, Kishimoto H, Kato A, Liu ACY, Suzuki K (2017) Effect of heating rate during primary crystallization on soft magnetic properties of melt-spun Fe-B alloys. *Scripta Mater* 132:68–72. <https://doi.org/10.1016/j.scriptamat.2017.01.030>
- [15] Fan XD, Zhang T, Jiang MF, Yang WM, Shen BL (2019) Synthesis of novel FeSiBPCCu alloys with high amorphous forming ability and good soft magnetic properties. *J Non-Cryst Solids* 503–504:36–43. <https://doi.org/10.1016/j.jnoncrystol.2018.09.021>
- [16] Li YH, Jia XJ, Xu YQ, Chang CT, Xie GQ, Zhang W (2017) Soft magnetic Fe-Si-B-Cu nanocrystalline alloys with high Cu concentrations. *J Alloy Compd* 722:859–863. <https://doi.org/10.1016/j.jallcom.2017.06.128>
- [17] Jia XJ, Li YH, Wu LC, Zhang Y, Xie L, Zhang W (2019) The role of Cu content on structure and magnetic properties of Fe-Si-B-P-Cu nanocrystalline alloys. *J Mater Sci* 54:4400–4408. <https://doi.org/10.1007/s10853-018-3131-5>
- [18] Hono K, Ping DH, Ohnuma M, Onodera H (1999) Cu clustering and Si partitioning in the early crystallization stage of an  $\text{Fe}_{73.5}\text{Si}_{13.5}\text{B}_9\text{Nb}_3\text{Cu}_1$  amorphous alloy. *Acta Mater* 47:997–1006. [https://doi.org/10.1016/S1359-6454\(98\)00392-9](https://doi.org/10.1016/S1359-6454(98)00392-9)
- [19] Matsuura M, Nishijing M, Takenaka K, Takeuchi A, Ofuchi H, Makino A (2015) Evolution of fcc Cu clusters and their structure changes in the soft magnetic  $\text{Fe}_{85.2}\text{Si}_{1.8}\text{B}_9\text{P}_4\text{Cu}_{0.8}$  (NANOMET) and FINEMET alloys observed by X-ray absorption fine structure. *J Appl Phys* 117:17A324. <https://doi.org/10.1063/1.491693>
- [20] Zuo MQ, Meng SY, Li Q, Li HX, Chang CT, Sun YF (2017) Effect of metalloid elements on magnetic properties of Fe-based bulk metallic glasses. *Intermetallics* 83:83–86. <https://doi.org/10.1016/j.intermet.2016.12.010>
- [21] Xu YQ, Li YH, Zhu ZW, Zhang W (2018) Formation and properties of  $\text{Fe}_{25}\text{Co}_{25}\text{Ni}_{25}(\text{P}, \text{C}, \text{B}, \text{Si})_{25}$  high-entropy bulk metallic glasses. *J Non-Cryst Solids* 487:60–64. <https://doi.org/10.1016/j.jnoncrystol.2018.02.021>
- [22] Hibino T, Bitoh T (2017) Ternary Fe-BC and quaternary Fe-BC-Si amorphous alloys with glass transition and high magnetization. *J Alloy Compd* 707:82–86. <https://doi.org/10.1016/j.jallcom.2016.12.060>
- [23] Zhang ZQ, Sharma P, Makino A (2012) Role of Si in high  $B_s$  and low core-loss  $\text{Fe}_{85.2}\text{B}_{10-x}\text{P}_4\text{Cu}_{0.8}\text{Si}_x$  nano-crystalline alloys. *J Appl Phys* 112:103902–103908. <https://doi.org/10.1063/1.4765718>
- [24] Li YH, Jia XJ, Zhang W, Zhang Y, Xie GQ, Qiu ZY, Luan JH, Jiao ZB (2020) Formation manner and crystallization behavior of Fe-based amorphous precursors with pre-existing  $\alpha$ -Fe nanoparticles. *J Mater Sci Technol*. <https://doi.org/10.1016/j.jmst.2020.05.049>
- [25] Suzuki K, Herzer G, Cadogan JM (1998) The effect of coherent uniaxial anisotropies on the grain-size dependence of coercivity in nanocrystalline soft magnetic alloys. *J Magn Magn Mater* 177:949–950. [https://doi.org/10.1016/S0304-853\(97\)00987-6](https://doi.org/10.1016/S0304-853(97)00987-6)

- [26] Herzer G (1990) Grain size dependence of coercivity and permeability in nanocrystalline ferromagnets. *IEEE Trans Magn* 26:1397–1402. <https://doi.org/10.1109/20.104389>
- [27] Jia XJ, Li YH, Wu LC, Zhang W (2020) A study on the role of Ni content on structure and properties of Fe-Ni-Si-B-P-Cu nanocrystalline alloys. *J Alloy Compd* 822(152784):152786. <https://doi.org/10.1016/j.jallcom.2019.152784>
- [28] Wu C, Chen HP, Lv HP, Yan M (2016) Interplay of crystallization, stress relaxation and magnetic properties for FeCuNbSiB soft magnetic composites. *J Alloy Compd* 673:278–282. <https://doi.org/10.1016/j.jallcom.2016.02.239>
- [29] Allia P (1993) Kinetics of the amorphous-to-nanocrystalline transformation in  $\text{Fe}_{73.5}\text{Cu}_1\text{Nb}_3\text{Si}_{13.5}\text{B}_9$ . *J Appl Phys* 74:3137–3143. <https://doi.org/10.1063/1.354581>
- [30] Wang WH (2007) Roles of minor additions in formation and properties of bulk metallic glasses. *Prog Mater Sci* 52:540–595. <https://doi.org/10.1016/j.pmatsci.2006.07.003>
- [31] Inoue A (2000) Stabilization of metallic supercooled liquid and bulk amorphous alloys. *Acta Mater* 48:279–306. [https://doi.org/10.1016/S1359-6454\(99\)00300-6](https://doi.org/10.1016/S1359-6454(99)00300-6)
- [32] Senkov ON, Miracle DB (2001) Effect of the atomic size distribution on glass forming ability of amorphous metallic alloys. *Mater Res Bull* 36:2183–2198. [https://doi.org/10.1016/S0025-5408\(01\)00715-2](https://doi.org/10.1016/S0025-5408(01)00715-2)
- [33] Takeuchi A, Inoue A (2000) Calculations of mixing enthalpy and mismatch entropy for ternary amorphous alloys. *Mater Trans JIM* 41:1372–1378. <https://doi.org/10.2320/matertrans1989.41.1372>
- [34] Takeuchi A, Inoue A (2005) Classification of bulk metallic glasses by atomic size difference, heat of mixing and period of constituent elements and its application to characterization of the main alloying element. *Mater Trans* 46:2817–2829. <https://doi.org/10.2320/matertrans.46.2817>
- [35] Zhang W, Jia XJ, Li YH, Fang CF (2014) Effects of Mo addition on thermal stability and magnetic properties of a ferromagnetic  $\text{Fe}_{75}\text{P}_{10}\text{C}_{10}\text{B}_5$  metallic glass. *J Appl Phys* 115:17A768–23. <https://doi.org/10.1063/1.4869161>
- [36] Ohta M, Yoshizawa Y (2009) High Bs nanocrystalline  $\text{Fe}_{84-x-y}\text{Cu}_x\text{Nb}_y\text{Si}_4\text{B}_{12}$  alloys ( $x = 0.0-1.4$ ,  $y = 0.0-2.5$ ). *J Magn Magn Mater* 321:2220–2224. <https://doi.org/10.1016/j.jmmm.2009.01.018>
- [37] Graham CD, Egami T (1979) Magnetic properties of amorphous ribbon. *IEEE Trans Mag* 15(6):1398–1403. <https://doi.org/10.1109/TMAG.1979.1060428>
- [38] Shi RM, Wang Z, Jia YY, Wen ZP, Wang BW, Zhang T (2012) Superior magnetic softness at elevated temperature of Si-rich Fe-based nanocrystalline alloy. *J Appl Phys* 112:083922–83924. <https://doi.org/10.1063/1.4759243>
- [39] Fan XD, Men H, Ma AB, Shen BL (2012) The influence of Si substitution on soft magnetic properties and crystallization behavior in  $\text{Fe}_{83}\text{B}_{10}\text{C}_{6-x}\text{Si}_x\text{Cu}_1$  alloy system. *Sci China Technol Sc* 55:2416–2419. <https://doi.org/10.1007/s11431-012-4929-z>
- [40] Sharma P, Zhang X, Zhang Y, Makino A (2014) Influence of microstructure on soft magnetic properties of low coreloss and high  $B_s$   $\text{Fe}_{85}\text{Si}_2\text{B}_8\text{P}_4\text{Cu}_1$  nanocrystalline alloy. *J Appl Phys* 115:17A340–23. <https://doi.org/10.1063/1.4868188>
- [41] Suzukia K, Herzer G (2012) Magnetic-field-induced anisotropies and exchange softening in Fe-rich nanocrystalline soft magnetic alloys. *Scripta Mater* 67:548–553. <https://doi.org/10.1016/j.scriptamat.2012.03.006>
- [42] Herzer G (2005) Anisotropies in soft magnetic nanocrystalline alloys. *J Magn Magn Mater* 294:99–106. <https://doi.org/10.1016/j.jmmm.2005.03.020>
- [43] Parsons R, Garitaonandia JS, Yanai T, Onodera K, Kishimoto H, Kato A, Suzuki K (2017) Effect of Si on the field-induced anisotropy in Fe-rich nanocrystalline soft magnetic alloys. *J Alloy Compd* 695:3156–3162. <https://doi.org/10.1016/j.jallcom.2016.11.330>
- [44] Tejedor M, GarcemHa JA, Carrizo J, Elbaile L, Santos JD (1999) Stress relief and magnetic properties of magnetostrictive  $\text{Fe}_{79}\text{B}_{16}\text{Si}_5$  amorphous magnetic ribbons. *J Magn Magn Mater* 202:485–491. [https://doi.org/10.1016/S0304-8853\(99\)00378-9](https://doi.org/10.1016/S0304-8853(99)00378-9)

**Publisher's Note** Springer Nature remains neutral with regard to jurisdictional claims in published maps and institutional affiliations.

## Terms and Conditions

Springer Nature journal content, brought to you courtesy of Springer Nature Customer Service Center GmbH (“Springer Nature”).

Springer Nature supports a reasonable amount of sharing of research papers by authors, subscribers and authorised users (“Users”), for small-scale personal, non-commercial use provided that all copyright, trade and service marks and other proprietary notices are maintained. By accessing, sharing, receiving or otherwise using the Springer Nature journal content you agree to these terms of use (“Terms”). For these purposes, Springer Nature considers academic use (by researchers and students) to be non-commercial.

These Terms are supplementary and will apply in addition to any applicable website terms and conditions, a relevant site licence or a personal subscription. These Terms will prevail over any conflict or ambiguity with regards to the relevant terms, a site licence or a personal subscription (to the extent of the conflict or ambiguity only). For Creative Commons-licensed articles, the terms of the Creative Commons license used will apply.

We collect and use personal data to provide access to the Springer Nature journal content. We may also use these personal data internally within ResearchGate and Springer Nature and as agreed share it, in an anonymised way, for purposes of tracking, analysis and reporting. We will not otherwise disclose your personal data outside the ResearchGate or the Springer Nature group of companies unless we have your permission as detailed in the Privacy Policy.

While Users may use the Springer Nature journal content for small scale, personal non-commercial use, it is important to note that Users may not:

1. use such content for the purpose of providing other users with access on a regular or large scale basis or as a means to circumvent access control;
2. use such content where to do so would be considered a criminal or statutory offence in any jurisdiction, or gives rise to civil liability, or is otherwise unlawful;
3. falsely or misleadingly imply or suggest endorsement, approval, sponsorship, or association unless explicitly agreed to by Springer Nature in writing;
4. use bots or other automated methods to access the content or redirect messages
5. override any security feature or exclusionary protocol; or
6. share the content in order to create substitute for Springer Nature products or services or a systematic database of Springer Nature journal content.

In line with the restriction against commercial use, Springer Nature does not permit the creation of a product or service that creates revenue, royalties, rent or income from our content or its inclusion as part of a paid for service or for other commercial gain. Springer Nature journal content cannot be used for inter-library loans and librarians may not upload Springer Nature journal content on a large scale into their, or any other, institutional repository.

These terms of use are reviewed regularly and may be amended at any time. Springer Nature is not obligated to publish any information or content on this website and may remove it or features or functionality at our sole discretion, at any time with or without notice. Springer Nature may revoke this licence to you at any time and remove access to any copies of the Springer Nature journal content which have been saved.

To the fullest extent permitted by law, Springer Nature makes no warranties, representations or guarantees to Users, either express or implied with respect to the Springer nature journal content and all parties disclaim and waive any implied warranties or warranties imposed by law, including merchantability or fitness for any particular purpose.

Please note that these rights do not automatically extend to content, data or other material published by Springer Nature that may be licensed from third parties.

If you would like to use or distribute our Springer Nature journal content to a wider audience or on a regular basis or in any other manner not expressly permitted by these Terms, please contact Springer Nature at

[onlineservice@springernature.com](mailto:onlineservice@springernature.com)